

Theoretical investigation of the high pressure structure, lattice dynamics, phase transition, and thermal equation of state of titanium metal

Cui-E Hu,^{1,2,a)} Zhao-Yi Zeng,^{1,2} Lin Zhang,^{1,b)} Xiang-Rong Chen,² Ling-Cang Cai,¹ and Dario Alfè³

¹National Key Laboratory for Shock Wave and Detonation Physics Research, Institute of Fluid Physics, Chinese Academy of Engineering Physics, Mianyang 621900, People's Republic of China

²Institute of Atomic and Molecular Physics, College of Physical Science and Technology, Sichuan University, Chengdu 610065, People's Republic of China

³Department of Earth Sciences and Department of Physics and Astronomy, Materials Simulation Laboratory and London Centre for Nanotechnology, University College London, Gower street, WC1E 6BT, London, United Kingdom

(Received 23 January 2010; accepted 24 March 2010; published online 4 May 2010)

We report a detailed first-principles calculation to investigate the structures, elastic constants, and phase transition of Ti. The axial ratios of both α -Ti and ω -Ti are nearly constant under hydrostatic compression, which confirms the latest experimental results. From the high pressure elastic constants, we find that the α -Ti is unstable when the applied pressures are larger than 24.2 GPa, but the ω -Ti is mechanically stable at all range of calculated pressure. The calculated phonon dispersion curves agree well with experiments. Under compression, we captured a large softening around Γ point of α -Ti. When the pressure is raised to 35.9 GPa, the frequencies around the Γ point along Γ -M-K and Γ -A in transverse acoustical branches become imaginary, indicating a structural instability. Within quasiharmonic approximation, we obtained the full phase diagram and accurate thermal equations of state of Ti. The phase transition ω -Ti \rightarrow α -Ti \rightarrow β -Ti at zero pressure occurs at 146 K and 1143 K, respectively. The predicted triple point is at 9.78 GPa, 931 K, which is close to the experimental data. Our thermal equations of state confirm the available experimental results and are extended to a wider pressure and temperature range. © 2010 American Institute of Physics. [doi:10.1063/1.3407560]

I. INTRODUCTION

The titanium group elements titanium (Ti), zirconium (Zr), hafnium (Hf), and their alloys have tremendous scientific and technological interest. These materials are very important in technology due to their mechanical strength, stiffness, resistance to degradation with rise in temperature, light weight, and corrosion resistance.¹ The scientific interest for these materials stem from the fact that they have a narrow d band in the midst of a broad sp band, which has an impact on their electronic and superconducting properties. The electronic transfer between the broad sp band and the narrow d band is the driving force behind many structural and electronic transitions in these materials.²⁻⁴ Ti can also be alloyed with other elements such as iron, aluminum, vanadium, and molybdenum, to produce strong lightweight alloys for aerospace, military, industrial processing, automotive, and other applications. As the mechanical properties depend upon the crystallographic phase, studies of the structural stability, phase diagram, and the mechanisms of the phase transformations have been vigorously pursued.⁵⁻¹²

At ambient condition, Ti is in the hexagonal-close-packed (hcp) crystal structure (α phase), and then transforms to a body-centered-cubic (bcc) structure (β phase) when the temperature is higher than 1155 K.¹² At room temperature, the α phase transforms to the hexagonal ω phase (three at-

oms per unit cell) when the pressure is increased. This α - ω transition is a representative example of martensitic transformations. The pressure driven α - ω transformation in pure Ti has significant technological implications in the aerospace industry because the phase formation lowers toughness and ductility.¹⁰ Recently, two high pressure phases γ -Ti (distorted hcp)¹¹ and δ -Ti (distorted bcc)⁵ have been found. Joshi *et al.*⁷ carried out total energy calculations employing the full-potential linear-augmented-plane wave (FPLAPW) method to examine the stability of the γ and δ phases with respect to the ω and β structures. They found that the γ phase observed in the experiments is a metastable phase that could be formed due to the shear stresses present in the experiments, and the δ phase is not at all stable at any compression.

The thermal properties and phase boundaries among α -, ω -, and β -Ti have attracted wide attention. But the complete pressure-temperature (P - T) phase diagram of Ti has not been well studied theoretically due to the well-known soften phonon modes of the β -Ti at low temperatures. Ostanin and Trubitsin⁹ first worked on the phase diagram of α -, ω -, and β -Ti using the Debye model. The fitting parameters of the ω -Ti were obtained without detailed justifications. Hennig *et al.* studied the P - T phase diagram of Ti using molecular dynamics (MD) simulations based on modified embedded atom potential.⁶ But the calculated α - β phase boundary is nearly independent on pressure, which is not consistent with the experimental results. Recently, Mei *et al.* also studied the

^{a)}Electronic mail: cuiehu@126.com.

^{b)}Electronic mail: zhanglinbox@263.net.

phase diagram using the combination of the density functional theory (DFT) and the Debye model. But they shifted the total energy of β -Ti down by 8 kJ mol⁻¹ artificially to match the experimental values, which should be treated with caution. Experimentally, the shock wave Hugoniot measurements showed that the metastable α -phase branched to 12 GPa where the transformation to the β -phase began.¹³ Zhang *et al.*¹⁴ reported the phase diagram of Ti using the synchrotron x-ray diffraction. And they showed that the equilibrium phase boundary of α - ω transition has a dT/dP slope of 345 K/GPa, which is much larger than all the previous results.^{12,15} In addition, during the α - ω transition, their associated entropy change is 0.57 J mol⁻¹ K⁻¹, which is also much smaller than the previous datum 1.49 J mol⁻¹ K⁻¹.¹⁵ By *in situ* high-pressure diffraction experiments, Zhang *et al.*¹⁶ also investigated the structural properties and thermal equation of state (EOS) of Ti up to 8.2 GPa and 900 K. The measured axial ratios (c/a) for both α - and ω -Ti remain constant over the experimental pressures, which is against the diamond anvil cells (DAC) results for α -Ti.¹⁷ These disputations still remain inconclusive and need to be clarified.

In our previous work,¹⁸ we only obtained the phase transition and EOS of α - and ω -Ti by using the Debye model. But in the present work, we describe a systematical investigation of the high pressure behaviors of Ti, including accurate structural and elastic properties, the phase diagram, and thermal EOS. The present investigation is more complete than our previous work.¹⁸ First-principles quantum-mechanical calculations have been very successful in predicting the phase stability and EOS for a wide class of crystals.¹⁹⁻²¹ Here, we first used static first-principles calculations within DFT to investigate the structural and elastic properties of Ti under high pressure. Then we employed the quasiharmonic approximation (QHA) to study the phase diagram, thermal EOS, and thermodynamic properties. The organization of this paper is as follows; Sec. II, we give a brief description of the theoretical computational methods. The results and discussions are presented in Sec. III. A short conclusion is drawn in Sec. IV.

II. DETAILS OF CALCULATIONS AND MODELS

The static calculations were based on the DFT, and performed with the VIENNA *AB INITIO SIMULATION PACKAGE*,²² using a highly accurate frozen core all-electron projector augmented wave method.²³ The exchange and correlation potentials were treated within the generalized gradient approximation of Perdew–Burke–Ernzerhof.²⁴ In order to avoid core overlap at high pressure, we treated semicore states 3s and 3p as valence electrons. This is at variance with our previous work,¹⁸ where we used a potential in which the valence electrons for Ti were in the 3d and 4s configuration. The plane-wave energy cutoff was 700 eV, which is much larger than 500 eV in the previous work. The calculations were conducted with 18×18×10, 12×12×18, 20×20×20, and 16×8×10 Γ -centered k meshes for α -, ω -, β -, and γ -Ti, respectively. All necessary convergence tests were performed and the self-consistence convergence of the energy was set to 10⁻⁶ eV/atom. To obtain the equilibrium struc-

tures of unit cells at applied pressures, internal atomic positions were optimized until the residual forces became less than 1×10⁻³ eV/Å. Phonon calculations were performed using the small displacement method.²⁵ The forces were obtained using first-principles calculations with 54, 81, and 64 atoms for α -, ω -, and β -Ti, respectively. To obtain the force constants for the phonon calculations, atomic displacements of 0.03 Å were employed.

The Helmholtz free energy F can be accurately separated as

$$F(V, T) = E_{\text{static}}(V) + F_{\text{phon}}(V, T) + F_{\text{elec}}(V, T), \quad (1)$$

where $E_{\text{static}}(V)$ is the energy of a static lattice at zero temperature T and volume V , $F_{\text{elec}}(V, T)$ is the thermal free energy arising from electronic excitations, and $F_{\text{phon}}(V, T)$ is the phonon contribution. Both $E_{\text{static}}(V)$ and $F_{\text{elec}}(V, T)$ can be obtained from static first-principles calculations directly. The phonon vibrational contribution $F_{\text{phon}}(V, T)$ has been calculated in the QHA

$$F_{\text{phon}}(V, T) = \frac{k_B T}{\Omega} \int_{\text{BZ}} dq \sum_s \ln[2 \sinh(\hbar \omega_{qs}/2k_B T)], \quad (2)$$

where $\Omega = (2\pi)^3/V$ is the volume of the Brillouin Zone (BZ), k_B is the Boltzmann constant, \hbar is the Plank constant divided by 2π , and ω_{qs} are the phonon frequencies. Unfortunately, within the present QHA, we are unable to obtain the free energy of β -Ti, since imaginary frequencies of the soft modes occur throughout the BZ. Though the β -Ti is unstable at zero temperature, it is stable when the temperature is higher than 1155 K.¹² Here we also assume that the β -Ti is stable at high temperature, and then we use the quasiharmonic Debye model^{26,27} to calculate vibrational Helmholtz free energies and other thermodynamic properties. By using this model, the vibrational contribution F_{vib} can be expressed as

$$F_{\text{vib}}(\Theta; T) = nk_B T \left[\frac{9}{8} \frac{\Theta}{T} + 3 \ln(1 - e^{-\Theta/T}) - D(\Theta/T) \right], \quad (3)$$

where n is the number of atoms per unit cell and $D(\Theta/T)$ is the Debye integral. The Debye temperature Θ is expressed by

$$\Theta = \frac{\hbar}{k_B} [6\pi^2 V^{1/2} n]^{1/3} f(\sigma) \sqrt{\frac{B_S}{M}}, \quad (4)$$

where M is the molecular mass per formula unit, B_S is the adiabatic bulk modulus, and $f(\sigma)$ is given by

$$f(\sigma) = \left\{ 3 \left[2 \left(\frac{2}{3} \frac{1+\sigma}{1-2\sigma} \right)^{3/2} + \left(\frac{1}{3} \frac{1+\sigma}{1-\sigma} \right)^{3/2} \right] - 1 \right\}^{1/3}, \quad (5)$$

where σ is the Poisson's ratio and can be obtained from the experimental elastic constants.²⁸ It is clear that once the parameters are defined, the Debye model can be used also in region where the β -Ti structure is not stable. We will do this later in the paper for completeness, but with the understanding that we will not assign any physical meaning to the properties obtained in this way.

The elastic constants are defined by means of a Taylor expansion of the total energy, $E(V, \delta)$, for the system with

TABLE I. The equilibrium axial ratio c/a , volume V_0 ($\text{\AA}^3/\text{atom}$), zero pressure bulk modulus B_0 (GPa), pressure derivative B' , B'' (1/GPa), and static energy E_0 (eV/atom).

		c/a	V_0	B_0	B'	B''	E_0
α	Present	1.583	17.38	110.02	3.59	-0.0477	-7.945
	Expt. (Ref. 17)	1.583	17.70 ± 0.05	117.0 ± 9.0	3.9 ± 0.4		
	Expt. (Ref. 11)	1.585	17.74	102.0	3.9		
	Expt. (Ref. 16)	1.587	17.64	114.0 ± 3.0	4.0		
ω	Present	0.618	17.14	110.51	3.60	-0.0462	-7.951
	Expt. (Ref. 17)	0.609	17.40 ± 0.08	138.0 ± 10.0	3.8 ± 0.5		
	Expt. (Ref. 11)	0.614	17.37	142.0	3.9		
	Expt. (Ref. 16)	0.613	17.29	107.0 ± 3.0	4.0		
β	Present		17.23	105.14	3.40	-0.0527	-7.836

respect to a small strain δ of the lattice primitive cell volume V . The energy of a strained system is expressed as follows:

$$E(V, \delta) = E(V_0, 0) + V_0 \left[\sum_i \tau_i \xi_i \delta_i + \frac{1}{2} \sum_{ij} C_{ij} \delta_i \xi_j \delta_j \right], \quad (6)$$

where $E(V_0, 0)$ is the energy of the unstrained system with equilibrium volume V_0 , τ_i is an element in the stress tensor, and ξ_i is a factor to take care of Voigt index.²⁹ For a cubic structure we considered three independent volume-nonconserving strains.^{30,31} A hexagonal crystal structure possesses five independent elastic constants, so we use five independent strains. The detailed accounts of the calculation method of the elastic constants have been reported in the previous calculations [hcp-Zr (Ref. 32) and bcc-Mo (Ref. 21)].

III. RESULTS AND DISCUSSION

A. Structural properties

To understand the properties of Ti at high pressure and temperature, we must know accurate information on the lattice structures first. We calculated the static energy-volume (E - V) curves for α -, ω -, β -, and γ -Ti. The equilibrium volume (V_0), the static energy (E_0), the bulk modulus (B_0), and its pressure derivative (B' and B'') of α -, ω -, and β -Ti, which are obtained by fitting the E - V data to the fourth-order finite strain EOS,³³ are listed in Table I. The agreement of our results with the experimental data^{11,16,17} is satisfactory. At zero pressure and temperature, the stable phase is ω -Ti. By comparing the enthalpies of α - and ω -Ti, we found that a transformation from the ω -Ti phase to the α -Ti phase would appear at a negative pressure of -5.0 GPa, which is consistent with other theoretical data -3.0 GPa (Ref. 34) and -3.7 GPa.³⁵ The equilibrium lattice parameters of γ -Ti are $a = 2.94$, $b = 5.09$, and $c = 4.65$ \AA . The bulk modulus B_0 and its pressure derivative B' are 105.43 GPa and 3.48 GPa, respectively. The phase transition from ω -Ti to γ -Ti occurs at 110 GPa, consistent with the experimental datum 116 ± 4 GPa.¹¹ At the transition pressure, the lattice parameters for γ -Ti are $a = 2.39$, $b = 4.51$, and $c = 3.96$ \AA , which also agree with the experimental data $a = 2.388$, $b = 4.484$, and $c = 3.915$ \AA at 118 GPa.¹¹ Meanwhile, the internal parameter varies from 0.166 at zero pressure to 0.108 at 110 GPa (the experimental datum is 0.10 at 118 GPa).¹¹ The calculated 0 K isotherms are

shown in Fig. 1, together with the experimental results.^{11,17} The present EOS agrees very well with the experimental data at all range of pressure.

At zero pressure and temperature, α -Ti has an axial c/a ratio of 1.583, smaller than the ideal value 1.633 for an hcp crystal. This behavior in hcp metals is generally attributed to highly anisotropic bonding properties, namely a strongly covalent bond character, with a component aligned along the c -axis.¹⁶ The pressure dependence of the lattice parameters and the corresponding c/a ratios for α - and ω -Ti are illustrated in Figs. 2(a) and 2(b). It can be seen that there are nearly identical axial compressibility along the a - and c -axis for α -Ti. As a result, the ratio c/a varies only slightly under pressure, indicating an isotropic compression, which confirms the latest experiment.¹⁶ But the DAC experiments revealed that the c/a ratio of the α -Ti increases gradually from 1.583 at atmospheric pressure to 1.622 at 14.5 GPa.¹⁷ For ω -Ti, the c/a ratio in the present work stays about constant to 0.617 at high pressure. From the experiments by Zhang *et al.*,¹⁶ we can see that the c/a ratio stays constant up to 8.2 GPa. Whereas, the c/a ratio in DAC experiments raises slightly from 0.609 at ambient pressure to 0.613 at 16 GPa.¹⁷ The increase in the c/a ratio (both for α - and ω -Ti) in the DAC experiments may be attributed to the uniaxial compression in nonhydrostatic conditions. Zhang *et al.* provided a

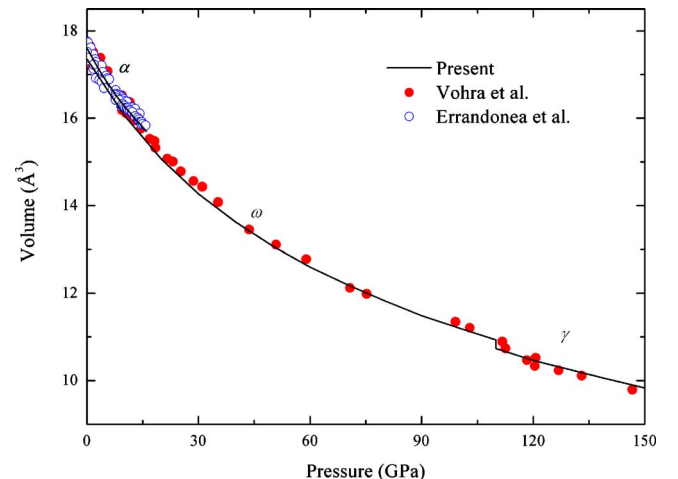


FIG. 1. (Color online) Zero temperature isotherms of Ti. The solid lines are the present work. The solid and open symbols are experimental data from Vohra and Spencer (Ref. 11) and Errandonea *et al.* (Ref. 17), respectively.

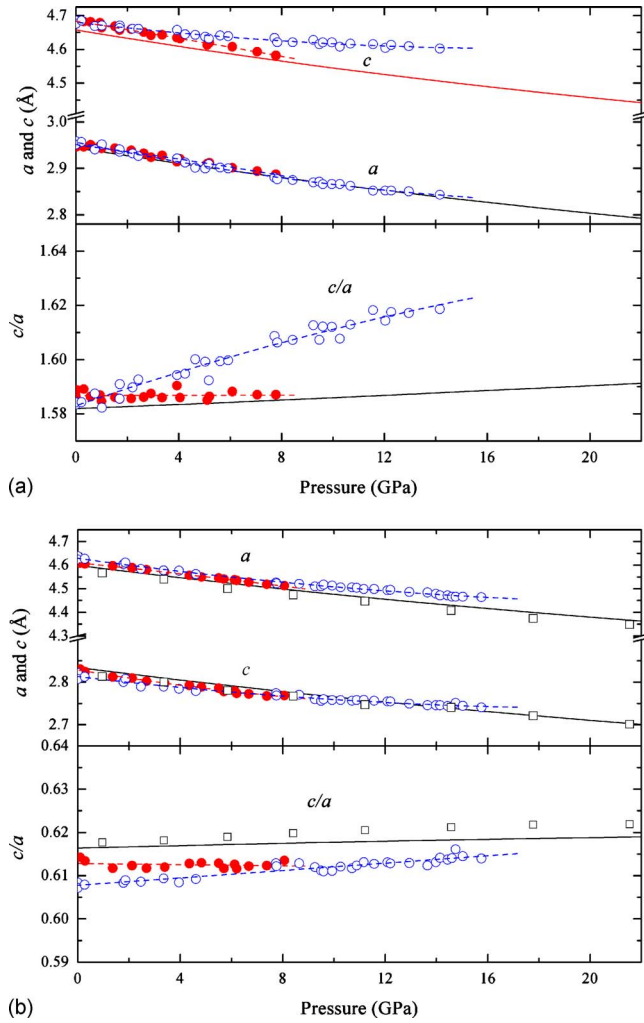


FIG. 2. (Color online) Lattice parameters a , c , and axial ratio c/a as a function of pressure for (a) α -Ti and (b) ω -Ti. The solid and open circles are the experimental data from Zhang *et al.* (Ref. 16) and Errandonea *et al.* (Ref. 17), respectively.

TABLE II. The calculated elastic modulus (GPa), Poisson's Ratio σ of Ti under pressure (GPa) at 0 K. The experimental data (Refs. 28 and 39) for α -Ti were measured at room pressure (RP) and 293 K, and for β -Ti were at 1273 K.

Ti	P	V/V_0	C_{11}	C_{12}	C_{13}	C_{33}	C_{44}	B	B_a	B_c	G	E	σ
α	0	1.00	175.0	82.6	74.7	196.0	41.8	112.1	324.3	363.4	41.0	109.7	0.337
	RP ^a		162.4	92.0	69.0	180.7	46.7						
	RP ^b							106.43			43.99	115.98	0.318
	3.56	0.97	186.2	96.5	85.9	215.0	41.7	124.7	356.5	415.1	40.7	110.0	0.353
	7.66	0.94	199.1	111.8	98.2	236.6	41.1	138.7	392.2	474.0	40.2	109.5	0.368
	12.38	0.91	207.8	132.9	111.1	258.0	39.8	153.3	430.2	533.3	37.0	102.8	0.388
	17.78	0.88	218.9	154.9	128.2	276.4	37.5	170.3	475.3	600.3	33.6	94.7	0.407
	23.95	0.85	230.4	180.3	147.4	288.8	33.9	188.5	531.5	648.1	28.7	82.0	0.427
ω	31.08	0.82	232.5	220.2	168.4	299.7	28.5	208.6	601.4	681.3	16.1	47.2	0.462
	0	1.00	199.2	81.5	50.4	247.1	54.8	112.1	326.8	357.3	53.7	138.9	0.293
	3.57	0.97	215.1	93.7	61.1	269.9	57.5	125.6	363.5	406.6	56.0	146.3	0.306
	7.70	0.94	232.9	107.7	71.6	293.5	60.1	139.9	404.3	454.4	58.4	153.7	0.317
	12.44	0.91	251.7	121.4	81.7	316.4	62.3	154.2	446.1	499.4	60.9	161.4	0.326
	17.87	0.88	274.8	136.8	95.3	343.9	64.2	171.8	496.3	558.4	64.0	170.8	0.334
	24.10	0.85	301.0	151.9	110.7	373.9	65.6	191.1	550.3	625.4	67.7	181.7	0.342
	31.37	0.82	330.1	168.9	128.1	405.3	66.3	212.5	611.2	697.6	71.4	192.7	0.349
β	0	1.00	91.8	114.4			40.8	106.9			-14.1	-44.4	0.569
	RP ^b		97.7	82.7			37.5	87.7					

^aReference 39.

^bReference 28.

uniform compression in all six directions of a cubic cell,¹⁶ which led a quasihydrostatic compression similar to the theoretical hydrostatic condition. Our results generally agree with theirs. The other available calculated results³⁵ are also shown in Fig. 2(b). For the similar hcp metal ω -Zr,³⁶ the calculations showed a constant axial ratio 0.623 at different pressures. In addition, in our previous calculations on ϵ -Fe, another hcp transition metal, we also found that the c/a ratio increases slightly (less than 0.01) with increasing pressure.³⁷ Experimentally, Weinberger *et al.*³⁸ investigated the hcp metal Os, and showed a nearly constant c/a ratio up to 30 GPa along hydrostatic stress conditions. So the constant c/a ratios under hydrostatic compression are reasonable properties in both α - and ω -Ti.

B. Elastic properties

For each volume of the unit cell, the complete sets of elastic constants of Ti were deduced from a polynomial fit of the strain energy for specific deformations. Ten symmetric values of γ in the range $\pm 5\%$ were used to make the strain energy fit at each strain type. For pressure, the value was calculated from the static EOS. The obtained elastic constants for α -, ω -, and β -Ti are listed in Table II, together with the experimental data.^{28,39} The elastic constants of α -Ti at equilibrium structure parameters are in good agreement with the experimental data with errors of less than 10%. Unfortunately, no experimental data for ω - and β -Ti at ambient condition are available for comparison. From Table II, one can see that all the elastic constants increase with increasing pressure except C_{44} of α -Ti.

The theoretical polycrystalline elastic modulus can be determined from an appropriate combination of elastic constants. The average isotropic bulk modulus B and shear modulus G of polycrystalline can be calculated according to

Voigt–Reuss–Hill approximations.⁴⁰ The polycrystalline Young's modulus (E) and the Poisson's ratio (σ) are then calculated from B and G as follows:

$$E = \frac{9BG}{3B + G}, \quad \sigma = \frac{3B - 2G}{2(3B + G)}. \quad (7)$$

To qualify the mechanical anisotropy of α - and ω -Ti, one can define bulk modulus along the a -axis (B_a) and the c -axis (B_c) as follows:⁴¹

$$B_a = a \frac{dp}{da} = \frac{\Lambda}{2 + \alpha}, \quad B_c = c \frac{dp}{dc} = \frac{B_a}{\alpha}, \quad (8)$$

$$\begin{aligned} \Lambda &= 2(C_{11} + C_{12}) + 4C_{13}\alpha + C_{33}\alpha^2, \quad \alpha \\ &= \frac{C_{11} + C_{12} - 2C_{13}}{C_{33} - C_{13}}. \end{aligned} \quad (9)$$

The values of B , B_a , B_c , G , E , and σ are also shown in Table II. Both G and E of α -Ti have the trend to decrease with the increasing pressure. In our calculated pressure range, the maximal change of B_a/B_c is 0.1 for α -Ti and 0.038 for ω -Ti, suggesting that the mechanical behavior of these two structures varies little under compression. This also confirms our results that the axial ratios of both α -Ti and ω -Ti are nearly invariant under compression. The Poisson's ratio of α -Ti increases more quickly than that of ω -Ti. At high pressure, the Poisson's ratio of α -Ti approaches to 0.5, which indicates the instability under compression. For the bcc structure β -Ti, we can see that the values of G and E are negative, indicating the instability. The Poisson's ratio is larger than the liquid value of 0.5, which is physically implausible since β -Ti is a solid.

For the cubic structure the mechanical stability under isotropic pressure can be judged by

$$\tilde{C}_{44} > 0, \quad \tilde{C}_{11} > |\tilde{C}_{12}|, \quad \tilde{C}_{11} + 2|\tilde{C}_{12}| > 0 \quad (10)$$

and for the hexagonal structure, the mechanical stability is judged by

$$\tilde{C}_{44} > 0, \quad \tilde{C}_{11} > |\tilde{C}_{12}|, \quad \tilde{C}_{33}(\tilde{C}_{11} + \tilde{C}_{12}) > 2\tilde{C}_{13}^2, \quad (11)$$

where

$$\tilde{C}_{\alpha\alpha} = C_{\alpha\alpha} - P(\alpha = 1, 3, 4), \quad \tilde{C}_{12} = C_{12} + P, \quad \tilde{C}_{13} = C_{13} + P. \quad (12)$$

We now apply the stability criterion for the three structures. For β -Ti the C_{11} is smaller than C_{12} , which indicates the β phase is unstable. For α -Ti, when the pressure is larger than 24.2 GPa at 0 K $\tilde{C}_{11} - |\tilde{C}_{12}| < 0$, which suggests that the α -Ti becomes mechanically unstable at this pressure. For the ω -Ti, we can see that it is stable in whole range of calculated pressures.

The isotropically averaged aggregate velocities can be obtained as follows:

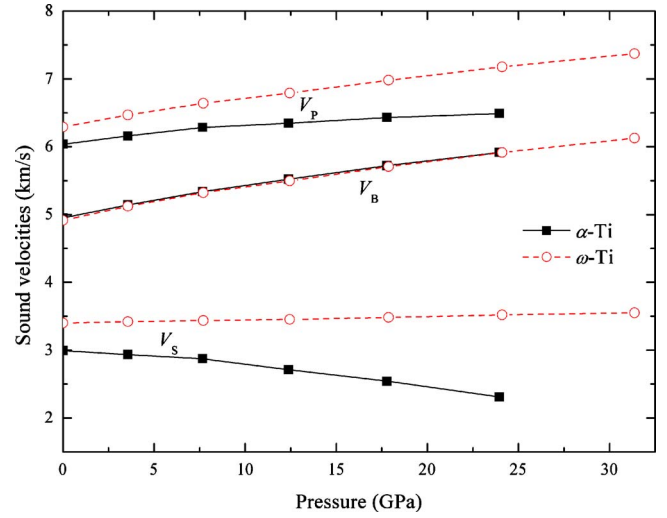


FIG. 3. (Color online) The aggregate sound velocities (V_P , V_B , and V_S) of α - and ω -Ti vs pressure at 0 K.

$$V_P = [(B + 4/3G)/\rho]^{1/2}, \quad V_B = (B/\rho)^{1/2}, \quad V_S = (G/\rho)^{1/2}, \quad (13)$$

where V_P , V_B , and V_S are the compressional, bulk, and shear sound velocities, respectively. The aggregate velocities versus pressure are shown in Fig. 3. As pressure increases, the V_B of α -Ti and ω -Ti are nearly equivalent and increase monotonically. At zero pressure, the V_P and V_S for α -Ti are smaller than those of ω -Ti. With increasing pressure, the V_P of ω -Ti increases with pressure significantly while the V_S increases only a little. For α -Ti, the V_S has a trend to decline. The softening of the V_S also indicates the instability of α -Ti under pressure.

C. Phonon dispersions

The calculated phonon dispersion curves of α -, ω -, and β -Ti along several symmetry directions at equilibrium structures are displayed in Figs. 4(a)–4(c). For α -Ti, the calculated phonon dispersion reproduces the overall trend of the inelastic-neutron-scattering measurement by Stassis *et al.*⁴² At the K point, the calculated high-energy optical frequencies show the largest deviations from experiment. However, the agreement of the acoustic branches is quite good. There are no experimental data available for high-pressure ω -Ti, but our results are consistent with some previous calculations.^{6,8} In contrast to α -Ti, the deviations for the optical branches of ω -Ti are smaller and more uniform across the BZ.

The predicted 0 K phonon dispersion of β -Ti is shown in Fig. 4(c), together with the experimental data measured at 1293 K.⁴³ The soft mode around P point in L-[111] is responsible for the β to ω transformation, while the unstable phonon branch in the T-[110] direction corresponds to the β to α transformation.⁴³ Though the present phonon dispersions reflect the instability, a large discrepancy exists. The reason is that the QHA only includes the part of anharmonic effects due to the volume dependence of the phonon frequencies, with the phonon frequencies at a given volume independent of temperature (a part from a possible dependence on the

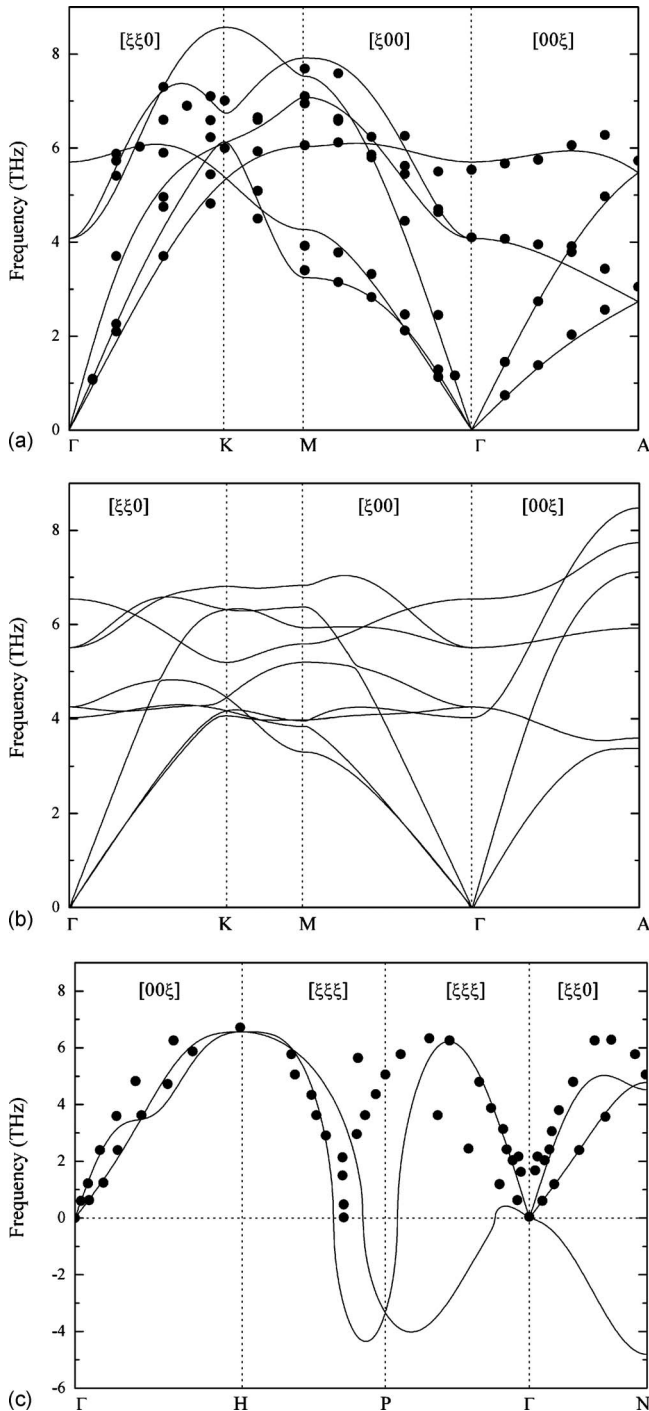


FIG. 4. Phonon dispersion curves of (a) α -, (b) ω -, and (c) β -Ti at 0 GPa and 0 K. The solid circles in (a) and (c) are the experimental data measured by Stassis *et al.* (Ref. 42) and Petry *et al.* (Ref. 43), respectively. The experimental data for β -Ti were measured at 1293 K.

electronic temperature). But in real crystals this is not the case. The effects of anharmonicity make each phonon frequency to suffer a shift. At high temperature, these shifts are proportional to the temperature and depend on frequencies.⁴³ There should be larger anharmonic effects when the temperature rises up to the α - β phase transition point.

We repeated the phonon calculations for other ten different pressures of both α - and ω -Ti. Some of the dispersion curves are plotted in Figs. 5(a) and 5(b). For ω -Ti, the phonon frequencies increase with increasing pressure. But for

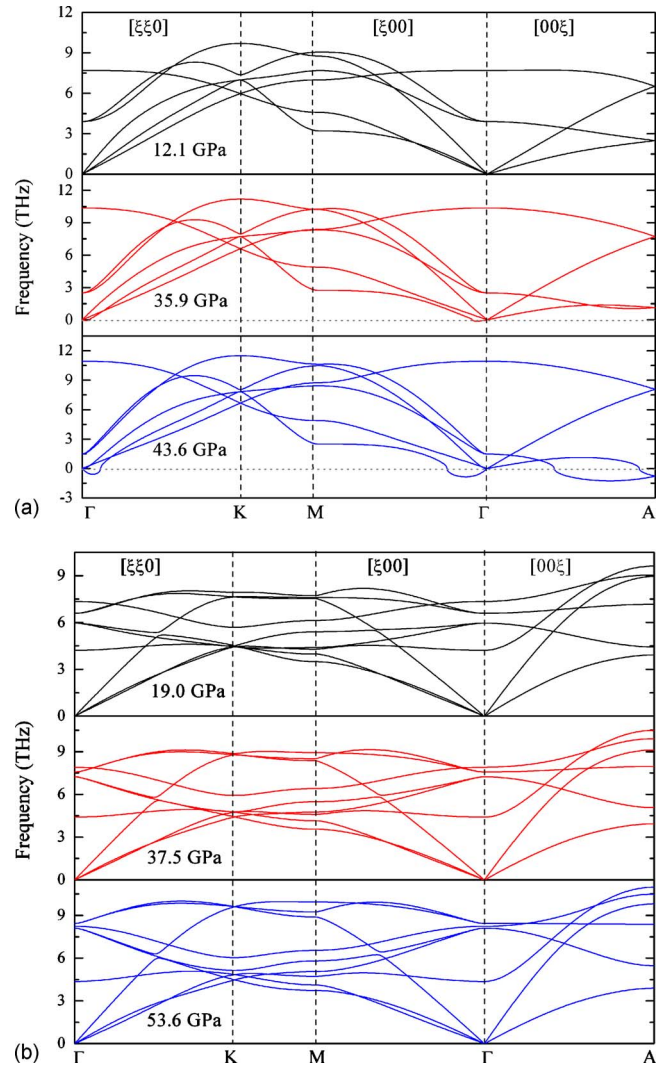


FIG. 5. (Color online) Phonon dispersion curves of (a) α -Ti and (b) ω -Ti at different pressures.

α -Ti, all the frequencies decrease with increasing pressure, except the highest-energy optical frequency. As pressure increases, the softening becomes more and more obvious. Under compression ($P=35.9$ GPa), the frequencies around the Γ point along Γ -M-K and Γ -A in the transverse acoustical (TA) branches soften to imaginary frequencies, indicating the structural instability. This is consistent with our static elastic constant calculations, where the α -Ti phase is unstable when the pressure is larger than 24.2 GPa. The modes softening behaviors are related to the particular mechanism which is responsible for the phase transition. For the β -Ti phase, the phonon dispersions at different pressures are not shown here, as the variations in the dispersion curves are mainly dependent on temperature and not on pressure.

The mode Grüneisen parameter $\gamma(q,j)$ describes the volume dependence of the frequency of the j th vibration mode of the lattice and is defined as

$$\gamma(q,j) = -d\{\ln[\omega(q,j)]\}/d[\ln \Omega]. \quad (14)$$

Figure 6 displays the dispersion curves of mode Grüneisen parameters of α - and ω -Ti along the high symmetry directions at 0 GPa. The mode Grüneisen parameters of ω -Ti are

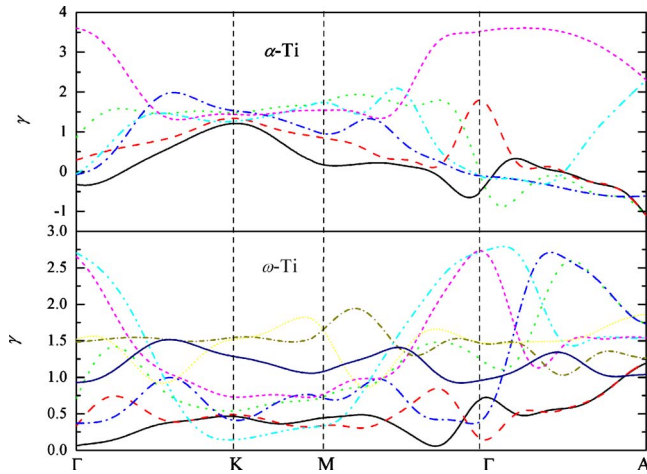


FIG. 6. (Color online) Mode Grüneisen parameter γ of α -Ti and ω -Ti at zero pressure.

positive throughout the whole BZ for all three branches. But there are several negative branches of α -Ti, especially along the Γ -A direction, which indicate the instability. It can be seen that the Grüneisen parameter is mode dependent and that the longitudinal modes are more sensitive to compression than the transverse ones.

D. Phase diagram

The difference of Gibbs free energy ΔG of ω - and β -Ti with respect to α -Ti can be obtained with two methods. The first is using the phonon density of states (DOS), and obtaining the free energy according to Eq. (2). Using this method, we find that the phase transition from ω -Ti to α -Ti occurs at 146 K at zero pressure. Since the phonon modes of β -Ti have imaginary frequencies, this prevents us from calculating the free energy using the DOS directly, so we need to employ the alternative approach of obtaining the free energy using the quasiharmonic Debye model. We can also calculate the free energies of α - and ω -Ti using this approach. Within the Debye model, the ω phase transforms to α phase at 152 K, and then transform to the β phase at 1143 K, which agree with the corresponding transition temperatures 186 and 1114 K from Mei *et al.*⁸ By comparing the Gibbs free energy of α -, ω -, and β -Ti at different pressures and temperatures, we can obtain the phase diagram of Ti. The full phase diagram of Ti is shown in Fig. 7, which generally agrees with previous theoretical^{6,8} and experimental^{12,14} data. The predicted triple point located at 9.78 GPa, 931 K, which is close to the experimental data 9 GPa, 940 K.¹²

At 300 K, the α - ω transition occurs at 2.02 GPa (using the phonon DOS) and 2.16 GPa (using the Debye model), which are in excellent agreement with experimental data 2.0 ± 0.3 GPa estimated from samples under shear stress.^{44,45} The slope (dT/dP) of the α - ω boundary (76 K/GPa from phonon DOS and 81 K/GPa from Debye model) is close to the previous studies from Young,¹² but significantly different from the findings by Zhang *et al.*¹⁴ (345 K/GPa). The experiments from Zhang *et al.* display a peculiar feature, i.e., if one extrapolates their α - ω phase boundary from 300 to 0 K, a wrong ground state would be found at

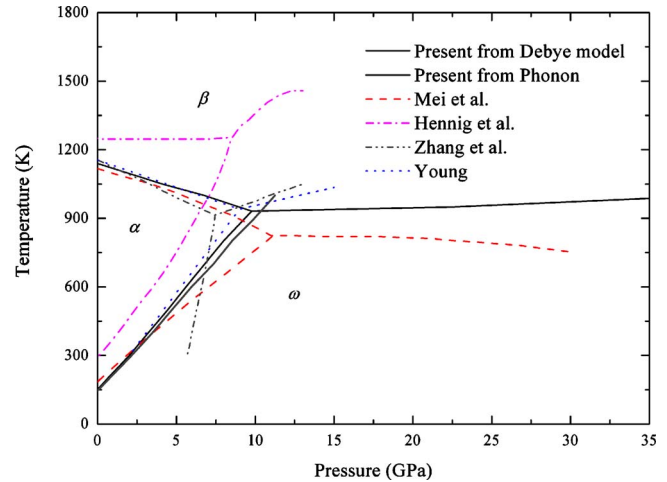


FIG. 7. (Color online) Phase diagram of Ti. The thin solid and thick grey lines are the present results. The dashed line and dashed-dotted line are the theoretical results from Mei *et al.* (Ref. 8) and Hennig *et al.* (Ref. 6), respectively. The dashed-dotted-dotted and dotted lines are the experimental data from Zhang *et al.* (Ref. 14) and Young (Ref. 12), respectively.

low temperature. Our slopes of the α - β and ω - β boundary are -21 K/GPa and 2.4 K/GPa, respectively. But Hennig *et al.*⁶ showed that the transition temperature between the α and β phase is nearly independent of pressure. Their classical MD results deviated from all other theoretical and experimental data, which could be due to transferability issues of their modified embedded atom model. The parameters were obtained by fitting energies, defect energies, forces, and elastic constants to DFT calculations at zero pressure and temperature. But the validity of those parameters at high pressure and temperature is unknown.

E. Thermal EOS

The thermal EOS is a measurement of the relationship among pressure, volume, and temperature (P - V - T). The calculated isotherms and isobars obtained by the quasiharmonic Debye approximation are compared with experiments in Figs. 8(a) and 8(b). The 0 K isotherm (including zero point motion) is almost the same as the one at 300 K and this is due to the small free energy contribution from the lattice vibrations at 300 K. At 300 K, the volume expands 0.61% (α -Ti) and 0.58% (ω -Ti) comparing with the corresponding static values. For α - and ω -Ti, our isotherms agree well with the experimental data with increasing pressure.¹⁶ The calculated volume of β -Ti at 1300 K and 0 GPa is 18.16 \AA^3 , which agrees well with the experimental data 18.13 \AA^3 [at 1273 K (Ref. 46)] and 18.22 \AA^3 [at 1293 K (Ref. 43)]. For the isobars, when the temperature goes from 0 to 1500 K at 0 GPa, the calculated volume expands about 5.73% (α -Ti) and 5.75% (ω -Ti). Under high pressure, the thermal expansion is suppressed quickly by pressure. Our isobar for ω -Ti at 8 GPa [the right panel of Fig. 8(b)] is consistent with the experimental data at 8.1 GPa.

The accurate thermodynamic properties as functions of pressure and temperature can directly provide the valuable information for understanding the phase diagram and the dynamical response of materials under extreme conditions. The

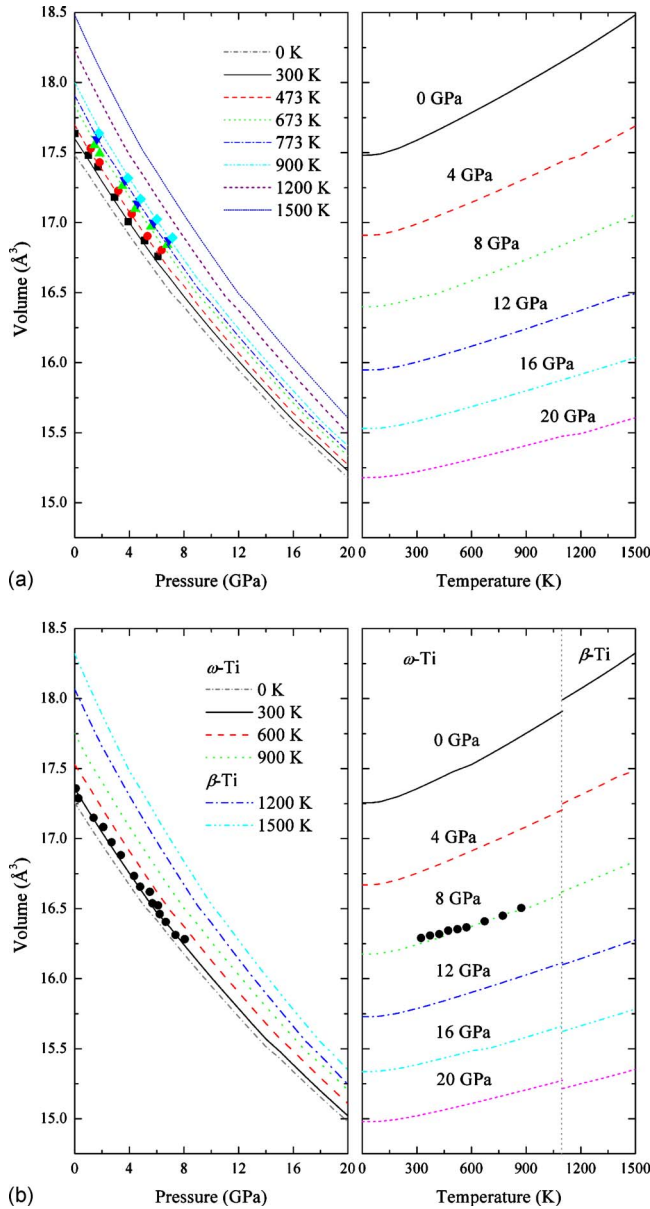


FIG. 8. (Color online) Thermal EOS of (a) α -, (b) ω -, and β -Ti, together with the experimental data (solid symbols) at the same condition (Ref. 16). The solid circles in the right plane of (b) are the experimental data at 8.1 GPa (Ref. 16), the grey line in the right plane of (b) locate at $T=1100$ K.

thermal pressure with respect to that of α -Ti at 300 K as functions of volume and temperature are shown in Fig. 9. At low temperature, the thermal pressures show little volume dependence. At elevated temperature, they clearly increase but only slightly with increasing volume. At the same condition, the thermal pressure of ω -Ti is larger than that of α -Ti and the thermal pressure of β -Ti is the smallest one. The calculated data by Zhang *et al.*¹⁶ at 900, 673, and 300 K for α -Ti are also shown in Fig. 9. Our results are larger than that of them. In addition, Zhang *et al.* considered that the thermal pressure is independent of volume and have the same constant slope of 0.00282 GPa/K for almost all the volumes. But in our calculations, the slopes increase from 0.0038, 0.0039, and 0.0036 at 16 \AA^3 to 0.0040, 0.0042, and 0.0039 at 18 \AA^3 for α -, ω -, and β -Ti, respectively. The behavior reported by Zhang *et al.*¹⁶ may be due to the inflexibility of their third

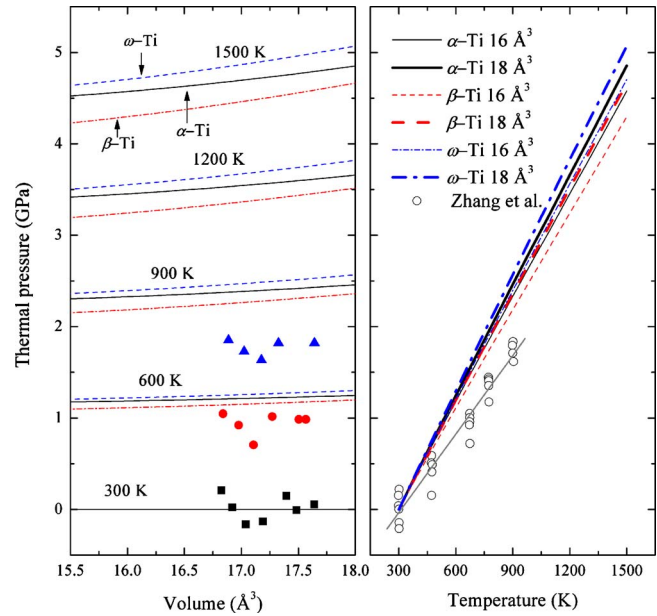


FIG. 9. (Color online) The thermal pressure as a function of volume and temperature. The solid triangles, circles, and squares in the left panel of the figure are the calculated data at 900, 673, and 300 K for α -Ti (Ref. 16). The grey line in the right panel of the figure is the linear fitted results for the calculated data (open circles) (Ref. 16).

order Birch–Murnaghan EOS in the calculations. The similar volume dependence of the slopes of the thermal pressure has also been found in our previous investigation on the bcc Mo.²¹ Meanwhile Sha and Cohen⁴⁷ and Liu *et al.*⁴⁸ also found that the slopes of the thermal pressure were strongly volume dependent for both bcc Fe and Ta.

The temperature and pressure dependences of B_T and B_S of Ti are illustrated in Figs. 10(a) and 10(b). The B_T and B_S are nearly constant from 0 to 100 K and then they decrease almost linearly with increasing temperatures. Our values for α -Ti are lower than the corresponding experimental ones.^{46,49} As temperature increases up to 1000 K, the deviation is about 3%. The reason for the difference is probably due to anharmonic effects in the thermal expansion. At 1300 K, the B_T of β -Ti is 83.6 GPa in the present work, which consists with the experimental datum 87.7 GPa at 1273 K.²⁸ At room temperature, the temperature derivative of B_T and B_S of α -Ti are -0.0175 GPa K^{-1} and -0.010 GPa K^{-1} , respectively. Our results agree with the datum $-0.011(7)$ GPa K^{-1} for B_T based on the measured P - V - T data.¹⁶ The first and second order pressure derivative of B_T (B' and B'') versus temperature and pressure are shown in Figs. 11(a) and 11(b), respectively. The first order pressure derivative B' increases with increasing temperature at a given pressure and decreases with increasing pressure at a given temperature. Whereas, the variation in the second order pressure derivative B'' is opposite to that of B' .

Figure 12 shows the entropy of Ti as functions of temperature and pressure. From Fig. 12(a), we can see that at the ω - α transition temperature 146 K, the entropy changes between the α - and ω -Ti is 1.3 J mol^{-1} K^{-1} , consistent with the datum 1.49 J mol^{-1} K^{-1} from previous study,¹⁵ but larger than the recent investigation 0.57 J mol^{-1} K^{-1} .¹⁴ The reason for the small value of 0.57 obtained by Zhang *et al.* is that

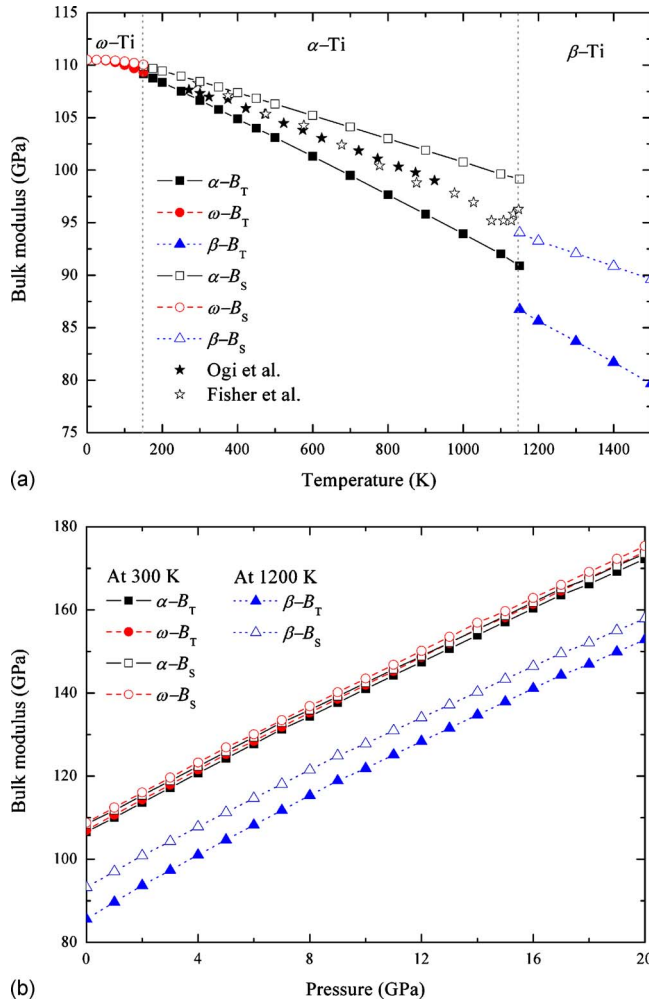


FIG. 10. (Color online) The isothermal bulk modulus B_T and adiabatic bulk modulus B_S vs (a) temperature at 0 GPa and (b) pressure. The solid and open stars are the experimental data from Ogi *et al.* (Ref. 46) and Fisher *et al.* (Ref. 49), respectively. The two grey vertical lines in (a), including Figs. 11(a) and 12(a), located at 146 K and 1143 K, respectively.

they calculated the entropy change using the Clausius–Clapeyron equation and the dT/dP of their α - ω boundary is too large. At the α - β transition temperature 1143 K, the entropy changes between the α - and β -Ti is $5.2 \text{ J mol}^{-1} \text{ K}^{-1}$, which is consistent with the experimental datum.⁵⁰ The large entropy change between the α - and β -Ti demonstrates that the α - β phase transition is driven by entropy. From Fig. 12(b), it is found that the entropy decrease with the increasing pressure and the entropy change among α -, ω -, and β -Ti keeps nearly constant at high pressure.

IV. CONCLUSIONS

We employed first-principles calculations to investigate the structures, elastic constants, and phase transitions of Ti. At zero pressure and temperature, the stable phase is ω -Ti and it transforms to γ -Ti at 110 GPa. The static EOS agrees with the experiments at all range of pressure. The axial ratios of both α -Ti and ω -Ti are nearly invariant under compression. From the high pressure elastic constants, we find that the α -Ti is unstable when the applied pressure is larger than 24.2 GPa, while the ω -Ti is mechanical stable at all range of

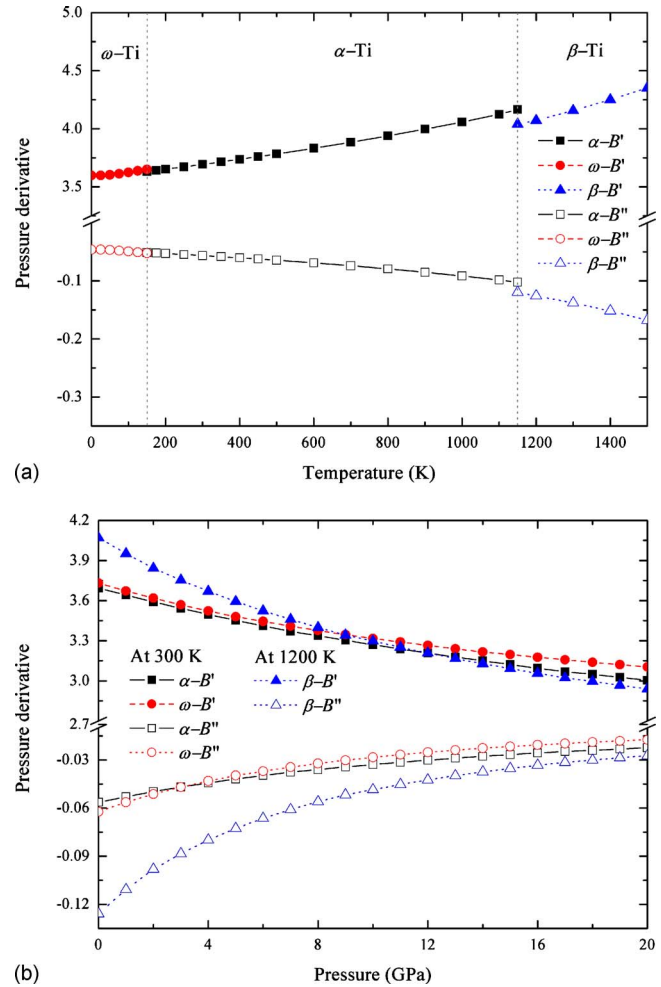


FIG. 11. (Color online) The first and second order pressure derivative of B_T (B' and B'') vs (a) temperature at 0 GPa and (b) pressure.

calculated pressures. The calculated phonon dispersion curves agree well with experiments. Under compression, we captured a large softening around the Γ point of α -Ti. As pressure increases, the softening becomes more and more obvious. When the pressure is raised to 35.9 GPa, the frequencies around the Γ point along Γ -M-K and Γ -A in the TA branches soften to imaginary frequencies, indicating a structural instability. For ω -Ti, all the frequencies are positive under pressure.

Within QHA, the phase boundary of α -Ti and ω -Ti from phonon DOS and quasiharmonic Debye model are consistent with each other. Based on the agreement of our calculated α - ω boundary with previous experiments and calculations, the full phase diagram and accurate thermal EOS of Ti are obtained. The phase transition ω -Ti \rightarrow α -Ti \rightarrow β -Ti at zero pressure occurs at 146 and 1143 K. The transition pressure from ω -Ti to α -Ti at 300 K is 2.02 GPa and the predicted triple point is at 9.78 GPa, 931 K, which is close to the experimental data. Thermodynamic properties are very important to extrapolate thermophysical properties to higher pressures and temperatures. We predicted the thermal EOS properties including isotherms, isobars, and thermal pressure, which confirmed the latest experimental results and were extended to a wider pressure and temperature range.

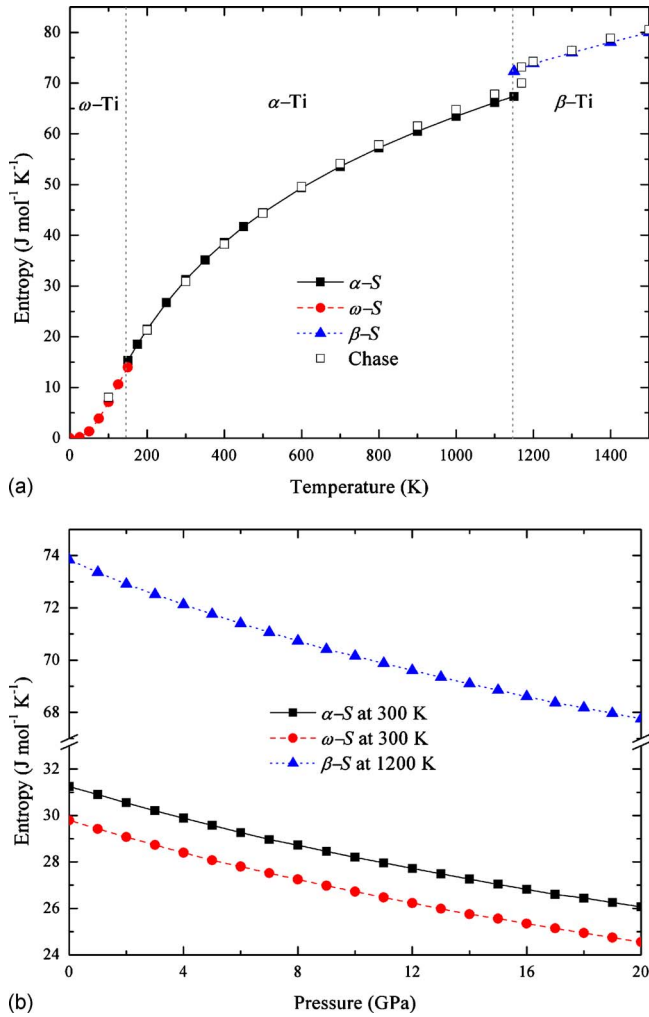


FIG. 12. (Color online) Entropy S of α -, ω -, and β -Ti as functions of (a) temperature at 0 GPa, compared with the experimental data from NIST-JANAF (open diamonds) (Ref. 50) and (b) pressure.

ACKNOWLEDGMENTS

The authors would like to thank Dr. Yan Bi for the helpful discussions. This research is supported by the National Key Laboratory Fund for Shock Wave and Detonation Physics Research under Grant Nos. 9140C6701010901 and 9140C6702030802, the National Natural Science Foundation of China under Grant Nos. 10776029 and 10776022.

¹C. Leyens and M. Peters, *Titanium and Titanium Alloys: Fundamentals and Applications* (Wiley, New York, 2003).

²J. Duthie and D. G. Pettifor, *Phys. Rev. Lett.* **38**, 564 (1977).

³J. S. Gyanchandani, S. C. Gupta, S. K. Sikka, and R. Chidambaram, *J. Phys.: Condens. Matter* **2**, 6457 (1990).

⁴H. L. Skriver, *Phys. Rev. B* **31**, 1909 (1985).

⁵Y. Akahama, H. Kawamura, and T. L. Bihan, *Phys. Rev. Lett.* **87**, 275503 (2001).

⁶R. G. Hennig, T. J. Lenosky, D. R. Trinkle, S. P. Rudin, and J. W. Wilkins, *Phys. Rev. B* **78**, 054121 (2008).

⁷K. D. Joshi, G. Jyoti, S. C. Gupta, and S. K. Sikka, *Phys. Rev. B* **65**, 052106 (2002).

⁸Z.-G. Mei, S.-L. Shang, Y. Wang, and Z.-K. Liu, *Phys. Rev. B* **80**, 104116 (2009).

⁹S. A. Ostanin and V. Y. Trubitsin, *J. Phys.: Condens. Matter* **9**, L491 (1997).

¹⁰S. Sikka, Y. Vohra, and R. Chidambaram, *Prog. Mater. Sci.* **27**, 245 (1982).

¹¹Y. K. Vohra and P. T. Spencer, *Phys. Rev. Lett.* **86**, 3068 (2001).

¹²D. A. Young, *Phase Diagrams of the Elements* (University of California Press, Berkeley, 1991).

¹³C. W. Greeff, D. R. Trinkle, and R. C. Albers, *J. Appl. Phys.* **90**, 2221 (2001).

¹⁴J. Zhang, Y. Zhao, R. S. Hixson, G. T. Gray III, L. Wang, W. Utsumi, S. Hiroyuki, and H. Takanori, *J. Phys. Chem. Solids* **69**, 2559 (2008).

¹⁵V. D. Blank and Y. S. Konyaev, *Fiz. Met. Metalloved* **53**, 402 (1982).

¹⁶J. Zhang, Y. Zhao, R. S. Hixson, G. T. Gray, L. P. Wang, W. Utsumi, S. Hiroyuki, and H. Takanori, *Phys. Rev. B* **78**, 054119 (2008).

¹⁷D. Errandonea, Y. Meng, M. Somayazulu, and D. Hausermann, *Physica B* **355**, 116 (2005).

¹⁸Y. J. Hao, L. Zhang, X. R. Chen, Y. H. Li, and H. L. He, *Solid State Commun.* **146**, 105 (2008).

¹⁹A. Kersch and D. Fischer, *J. Appl. Phys.* **106**, 014105 (2009).

²⁰Q. Liu, C. Fan, and R. Zhang, *J. Appl. Phys.* **105**, 123505 (2009).

²¹Z.-Y. Zeng, C.-E. Hu, L.-C. Cai, X.-R. Chen, and F.-Q. Jing, *J. Phys. Chem. B* **114**, 298 (2010).

²²G. Kresse and J. Furthmüller, *Phys. Rev. B* **54**, 11169 (1996).

²³P. E. Blöchl, *Phys. Rev. B* **50**, 17953 (1994).

²⁴J. P. Perdew, K. Burke, and M. Ernzerhof, *Phys. Rev. Lett.* **77**, 3865 (1996).

²⁵D. Alfè, *Comput. Phys. Commun.* **180**, 2622 (2009).

²⁶M. A. Blanco, A. M. Pendás, E. Francisco, J. M. Recio, and R. Franco, *J. Mol. Struct.: THEOCHEM* **368**, 245 (1996).

²⁷M. Flórez, J. M. Recio, E. Francisco, M. A. Blanco, and A. M. Pendás, *Phys. Rev. B* **66**, 144112 (2002).

²⁸H. Ledbetter, H. Ogi, S. Kai, S. Kim, and M. Hirao, *J. Appl. Phys.* **95**, 4642 (2004).

²⁹L. Fast, J. M. Wills, B. Johansson, and O. Eriksson, *Phys. Rev. B* **51**, 17431 (1995).

³⁰G. V. Sin'ko, *Phys. Rev. B* **77**, 104118 (2008).

³¹G. V. Sin'ko and N. A. Smirnov, *J. Phys.: Condens. Matter* **14**, 6989 (2002).

³²Y.-J. Hao, L. Zhang, X.-R. Chen, Y.-H. Li, and H.-L. He, *J. Phys.: Condens. Matter* **20**, 235230 (2008).

³³F. Birch, *J. Geophys. Res.* **91**, 4949 (1986).

³⁴A. L. Kutepov and S. G. Kutepova, *Phys. Rev. B* **67**, 132102 (2003).

³⁵Z.-G. Mei, S. Shang, Y. Wang, and Z.-K. Liu, *Phys. Rev. B* **79**, 134102 (2009).

³⁶W. Liu, B. Li, L. Wang, J. Zhang, and Y. Zhao, *Phys. Rev. B* **76**, 144107 (2007).

³⁷Z.-Y. Zeng, Z.-L. Liu, X.-R. Chen, L.-C. Cai, and F.-Q. Jing, *Chin. Phys. Lett.* **25**, 1757 (2008).

³⁸M. B. Weinberger, S. H. Tolbert, and A. Kavner, *Phys. Rev. Lett.* **100**, 045506 (2008).

³⁹G. Simmons and H. Wang, *Single Crystal Elastic Constants and Calculated Aggregate Properties: A Handbook*, 2nd ed. (MIT Press, Cambridge, 1971).

⁴⁰R. Hill, *Proc. Phys. Soc. Lond.* **65**, 350 (1952).

⁴¹P. Ravindran, L. Fast, P. A. Korzhavyi, B. Johansson, J. M. Wills, and O. Eriksson, *J. Appl. Phys.* **84**, 4891 (1998).

⁴²C. Stassis, D. Arch, and B. N. Harmon, *Phys. Rev. B* **19**, 181 (1979).

⁴³W. Petry, A. Heiming, J. Trampenau, M. Alba, C. Herzig, H. R. Schober, and G. Vogl, *Phys. Rev. B* **43**, 10933 (1991).

⁴⁴V. A. Zilbershtein, N. P. Chistotina, A. A. Zharov, N. A. Grishina, and E. I. Estrin, *Fiz. Met. Metalloved.* **39**, 445 (1975).

⁴⁵V. A. Zilbershteyn, G. I. Nosova, and E. I. Estrin, *Fiz. Met. Metalloved* **35**, 584 (1973).

⁴⁶H. Ogi, S. Kai, H. Ledbetter, R. Tarumi, M. Hirao, and K. Takashima, *Acta Mater.* **52**, 2075 (2004).

⁴⁷X. Sha and R. E. Cohen, *Phys. Rev. B* **73**, 104303 (2006).

⁴⁸Z.-L. Liu, L.-C. Cai, X.-R. Chen, Q. Wu, and F.-Q. Jing, *J. Phys.: Condens. Matter* **21**, 095408 (2009).

⁴⁹E. S. Fisher and C. J. Renken, *Phys. Rev.* **135**, A482 (1964).

⁵⁰M. W. Chase, *NIST-JANAF Thermochemical Tables* (American Institute of Physics, Washington, DC, 1998).